SUPPLEMENTAL INFORMATION

Contact efficiency optimization for tribovoltaic nanogenerator

Zhihao Zhao,[ab‡] Jiayue Zhang,[ac‡] Wenyan Qiao,[ab‡] Linglin Zhou,[ab] Ziting Guo,[ab] Xinyuan Li,[ab] Zhong Lin Wang,*[ade] Jie Wang*[ab]

a. Beijing Institute of Nanoenergy and Nanosystems, Chinese Academy of Sciences, Beijing 100083, P. R. China.

b. School of Nanoscience and Engineering, University of Chinese Academy of Sciences, Beijing 100049, P. R. China.

c. Department of Mechanical Engineering, Tsinghua University, Beijing 100084, P. R. China.

d. Yonsei Frontier Lab, Yonsei University, Seoul 03722, Republic of Korea.

e. School of Materials Science and Engineering, Georgia Institute of Technology, Atlanta, GA 30332, USA.

‡ The authors contributed equally to this work.

*Corresponding Author:

Z. L. Wang: zhong.wang@mse.gatech.edu; J. Wang: wangjie@binn.cas.cn

CONTENTS

Figure S22. The short-circuit current, transferred charges, and open-circuit voltage of non-optimized TVNG under different sliding acceleration.

Figure S23. The energy density of non-optimized TVNG, sliding-mode TENG, and O-TVNG under matched resistance, respectively.

Figure S24. The schematic diagram of sliding-mode TENG.

Figure S25. The scanning electron micrographs of silicon surface.

Figure S26. XRD patterns of silicon for TVNG before/after stability test.

Figure S27. The XPS spectra of silicon surface.

Figure S28. The Cu2p spectra and Si2p spectra of silicon for TVNG before/after the stability test.

Supplementary Tables

Table S1. The turn-on voltage of TVNG under different pressure force.

Table S2. The voltage (E_Q), current (I_Q) and resistance (R_Q) of quiescent operation point under different Cu areas.

Table S3. The average R_Q of quiescent operation point under different Cu areas.

Table S4. The R_Q, $R_{c,Cu}$, A_{eff}, and contact resistivity of TVNG device with/without interface optimization under different loading force.

Supplementary Notes

Note S1: The relationship between contact resistance and effective contact area for TVNG.

Note S2: The calculation of resistance of TVNG in quiescent operation point.

Note S3: The influence of surface roughness on contact condition of TVNG.

Note S4: The contact condition between Ga-In liquid metal and p-type silicon.

Note S5: The difference of contact condition between TVNG with and without interface optimization methods.

Note S6: Contribution of the friction between MoS_2 and Cu/silicon, and the friction between liquid and Cu/silicon for the output of TVNG.

Note S7: The design optimization strategy for TVNG device.

Note S8: The surface characteristics of silicon before/after long-term operation.

EXPERIMENTAL SECTION

Materials

The p-type silicon wafers (1-20 Ω cm) were purchased from Zhejiang Lijing Photoelectric Technology Co., LTD, which is a crystal planar oriented along [100], with a diameter of 100 ± 0.4 mm, a thickness of 500 ± 10 μm, and a tiny surface roughness of 0.5 ± 0.01 nm. Copper foil is commercial copper foil with a thickness of 50 μm. The MoS_2 suspension liquid (concentration: 1 mg/ml) was purchased from Nanjing BG Electronic Tech. Co., LTD. The MoS_2 was prepared by the Liquid phase stripping method with a thickness of 1-10 MoS_2 layers and size ranging from 0.05 to 1 μm, which was dispersed in a mixture of ethanol and water.

Fabrication of TVNG device

The Au electrode was supered on the back of the p-type silicon wafer as the bottom electrode, and the wafer was cut into a rectangle of 2 × 4 cm as a stator by a glass knife. The slider is Cu electrode: the acrylic with the thickness of 5 mm was cut into small squares with 10 × 10 mm as substrate by a laser cutting machine (PLS6.75 universal laser system), the copper foil was adhered on the polished substrate, and the wire was connected on the copper foil. To obtain the Cu electrode slider with microstructural channeling grooves, the acrylic with the thickness of 5 mm was cut into a 10 × 20 mm rectangle, the patterned channeling grooves were prepared by laser engraving and ensured that the area of the projecting portion was 1 cm^2. The width of each projecting portion and undercut part was equal, which was ranging from 2 mm to 0.25 for different samples. Then, the copper foil was adhered on the polished substrate with channeling grooves, and the copper foil on the undercut part was pressed and adhered on the bottom to ensure it could not contact with p-type silicon. The wire was connected to the copper foil. For the p-type silicon with different surface roughness, the sandpapers with different meshes were utilized to polish the Cu and p-type silicon for 10 cycles under the loading force of 10 N, respectively.

Characterization and electrical measurement

The short-circuit current and open-circuit voltage of TVNG are tested by a programmable electrometer (6514, Keithley Instruments model). A linear motor (TSMV120-1S, LinMot) is used to achieve the sliding movement processes, unless the text states otherwise, the sliding distance is 1 cm, the pressure is 10 N, the slider slides with a constant speed of 0.01 m s^{-1}, dwell time between two movements is 1 s. Precision source/measure units (B2902B, Keysight) are used to test the current *vs*. voltage curve of TVNG, and the voltage is increased gradually from -5.0 V to 5.0 V with a step of 10 mV, and at least 3 samples are tested. The Au electrode and Cu electrodes with standard areas are sputtered by Denton magnetron sputtering coating apparatus (Discovery 635) with a thickness of ~0.85 μm. Scanning electron microscopy (S4800, Hitachi) is used to measure the micrographs of silicon. X-ray diffraction (XRD) powder test equipment (X'pert3 Powder) is used to measure the XRD patterns of silicon. A spectrometer (Thermo Scientific K-Alpha) equipped with a monochromatic Al Kα X-ray source (1486.68 eV) is used to measure the X-ray photoelectron spectroscopy (XPS) under vacuum ($P < 10^{-9}$ mbar) with a pass energy of 200 eV (survey scans) or 50 eV (high-resolution scans). The Surface roughness measuring instrument (TR210, JIMTEC) is used to test the surface roughness value of silicon. Three-dimensional surface topographies of the samples are measured with a white light interferometer (Contour X200, Bruker). The conductivity of the interface optimization liquids is tested through the DDSJ-308A (REX) liquid conductivity meter.

Supplementary Figures, Tables and Notes

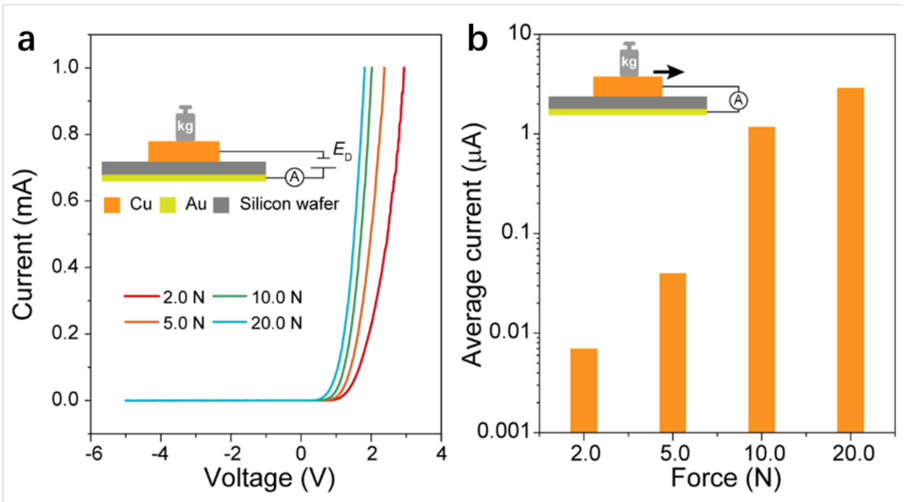

Figure S1. (a) *I-V* curves of TVNG under different loading forces (the insert is the schematic of the circuit). (b) Output average current of TVNG under different loading forces (the insert is the schematic of the circuit).

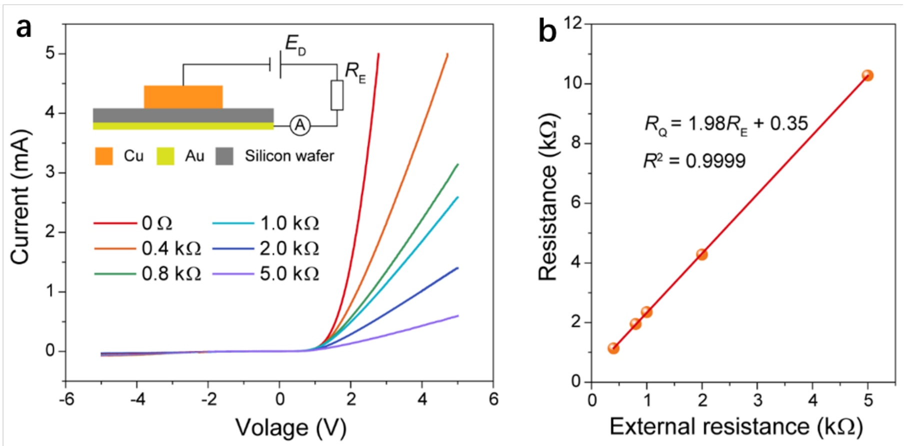

Figure S2. (a) *I-V* curves of TVNG with various external resistance (the insert is the schematic of the circuit). (b) Fitting curve of quiescent resistance *vs*. external resistance.

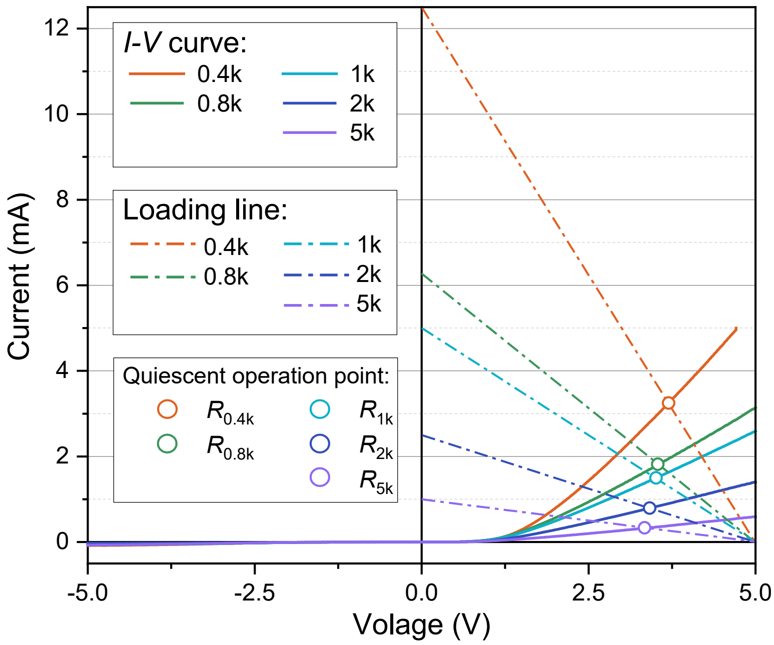

Figure S3. The *I-V* curves and quiescent operation points under different external resistances of 0.4 kΩ, 0.8 kΩ, 1 kΩ, 2 kΩ, and 5 kΩ, respectively.

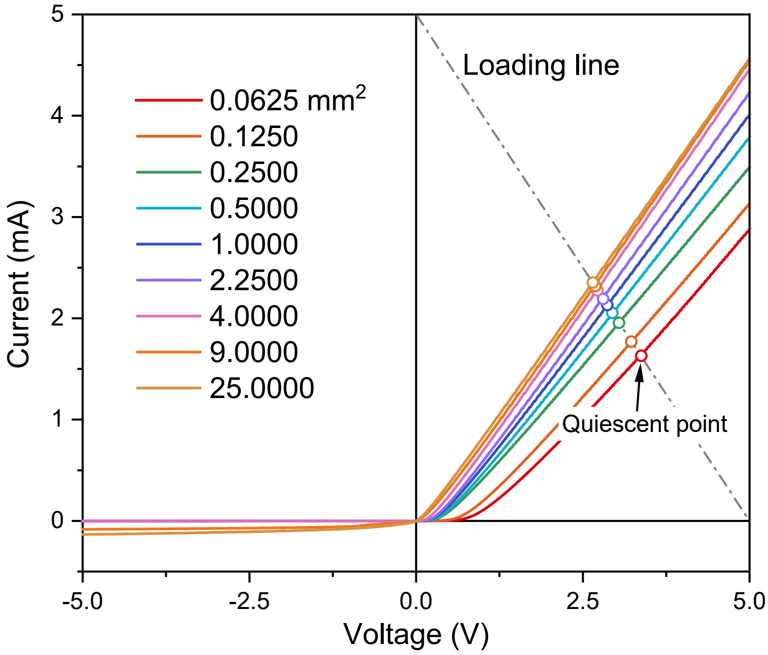

Figure S4. The *I-V* curves and quiescent operation points under different sputtering Cu areas.

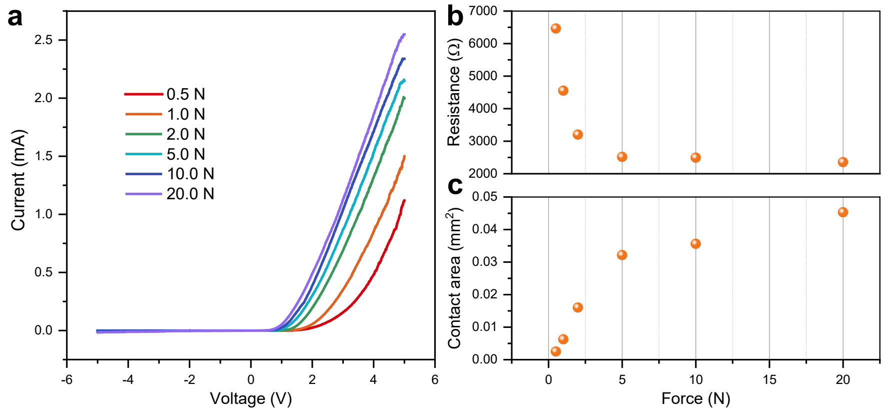

Figure S5. The (a) *I-V* curves and corresponding (b) resistance and (c) contact area of TVNG under different pressure force.

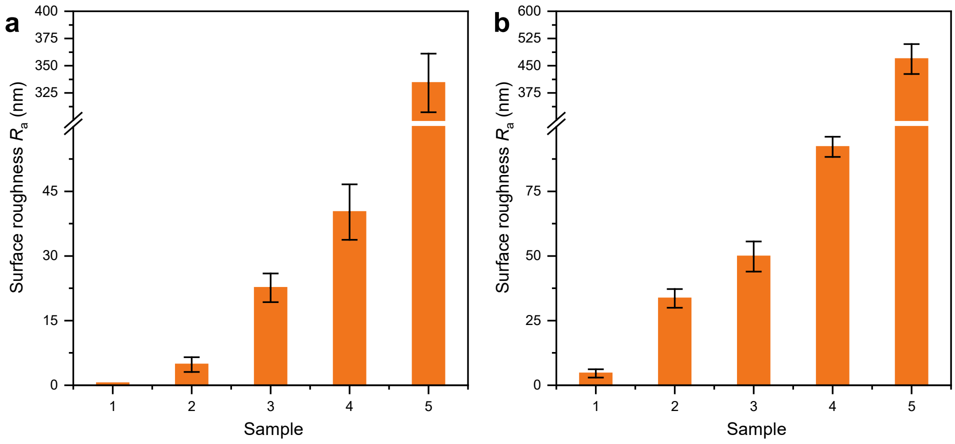

Figure S6. The surface roughness of (a) silicon and (b) Cu electrode.

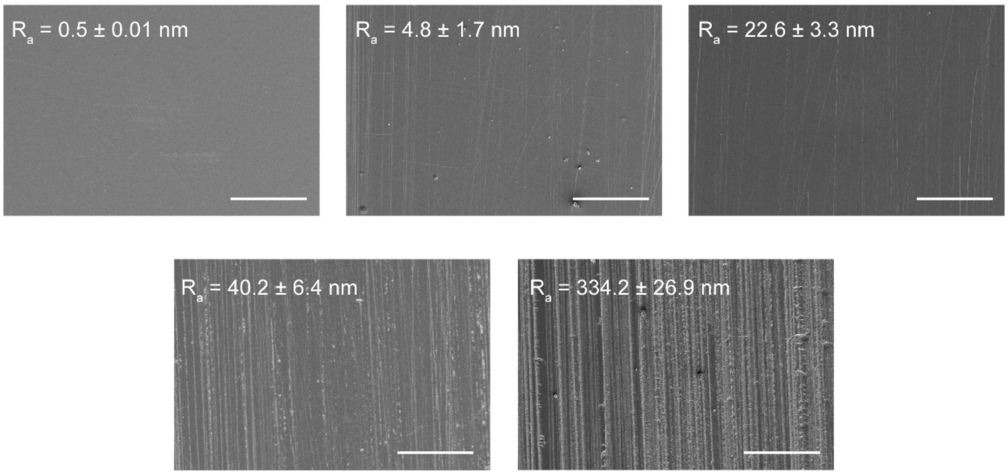

Figure S7. The micrographs of silicon with different surface roughness (scale bar: 30 μm).

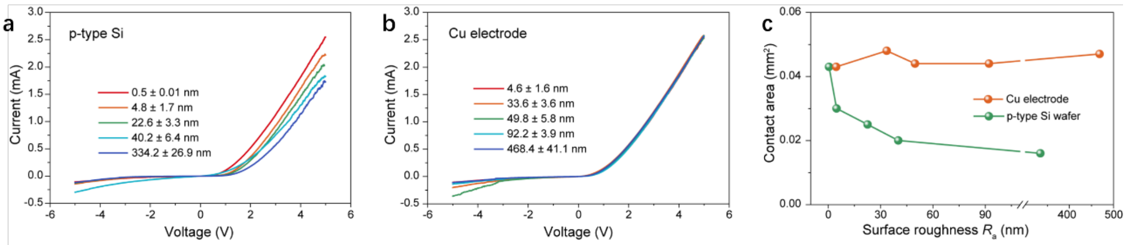

Figure S8. *I*-*V* curves of TVNG with different surface roughness of (a) p-type silicon and (b) Cu electrode. (c) Contact area of TVNG with different surface roughness.

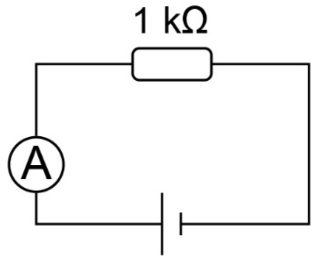

Figure S9. The circuit that tests the *I*-*V* curve of 1 kΩ.

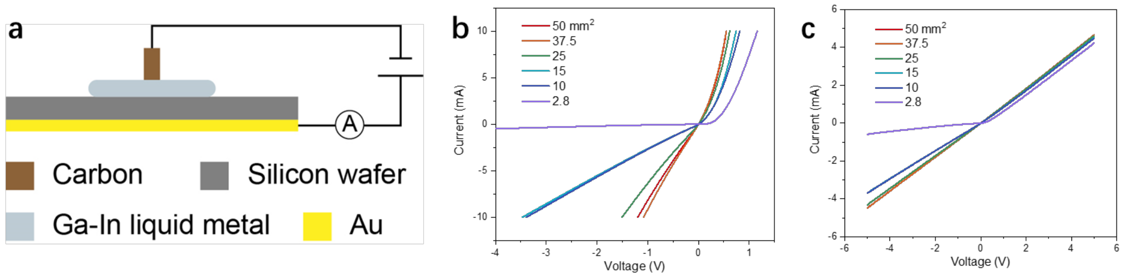

Figure S10. (a) Schematic of the circuit for the *I-V* test. (b) *I-V* curves of the Ga-In liquid metal and the p-type silicon with various area sizes of Ga-In. (c) *I-V* curves of the Ga-In liquid metal and the p-type silicon with various area sizes of Ga-In under external resistance of 1 kΩ.

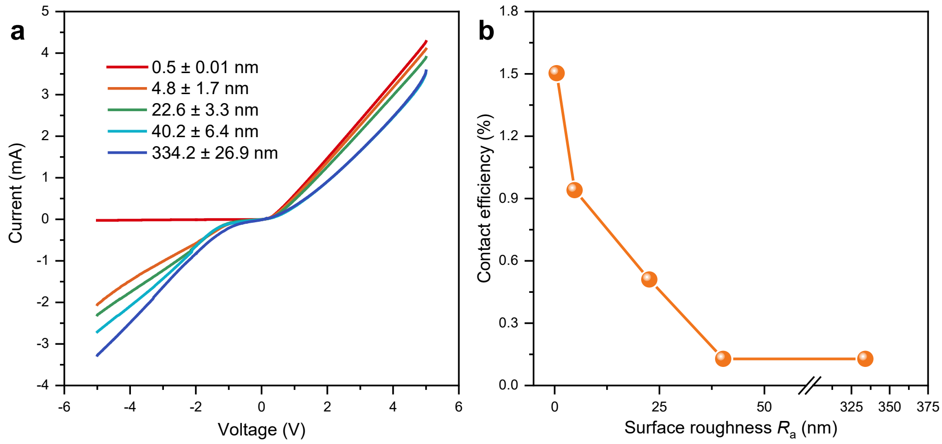

Figure S11. The (a) *I-V* curves and (b) corresponding contact efficiency of TVNG with different surface roughness of p-type silicon (the content of MoS_2 (sl) is 5 μL).

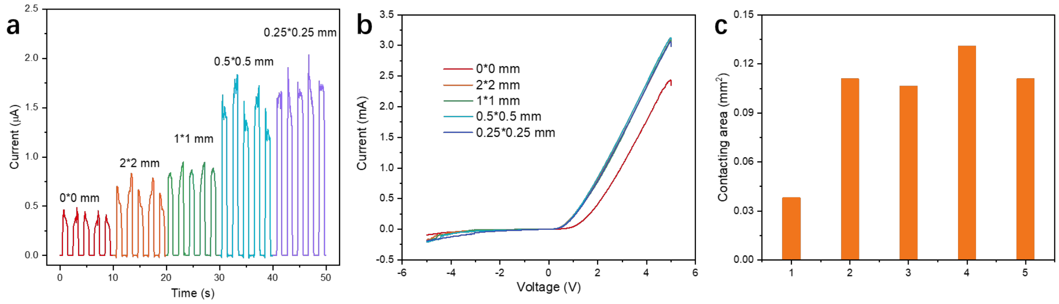

Figure S12. The (a) short-circuit current of TVNG devices with different microstructural channeling grooves. The (b) *I-V* curves and (c) corresponding contact area of TVNG with different microstructural channeling grooves.

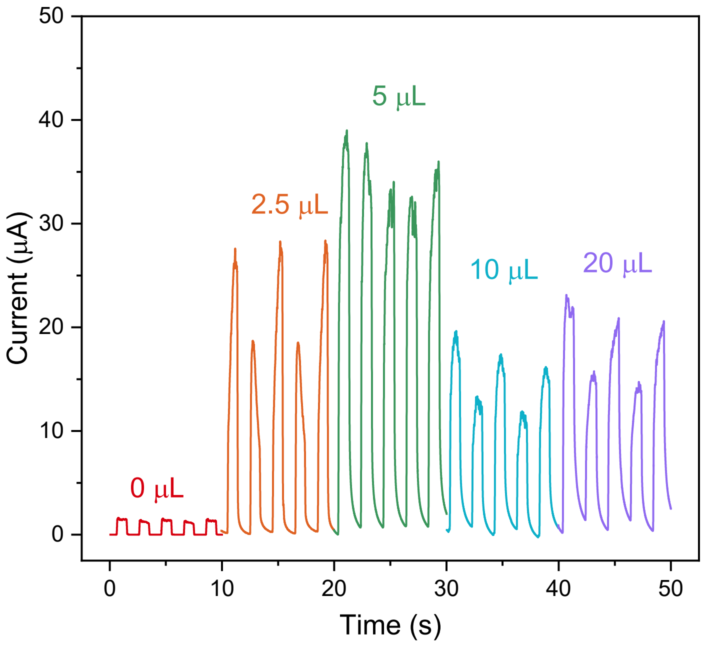

Figure S13. The short-circuit current of TVNG with channeling groove of 0.5 × 0.5 mm under different content of MoS_2 suspension liquid (sliding distance: 1 cm).

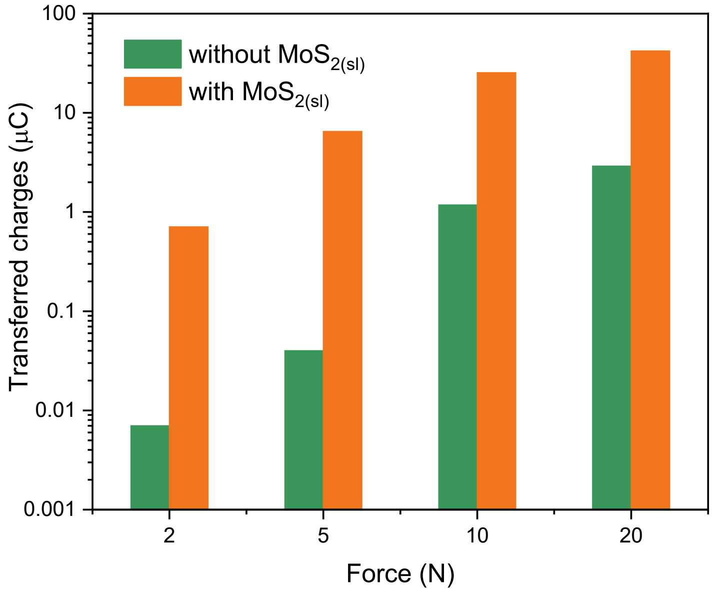

Figure S14. The short-circuit current of TVNG with channeling groove of 0.5 × 0.5 mm under different pressure force (MoS_2 suspension liquid: 5 μL, sliding distance: 1 cm).

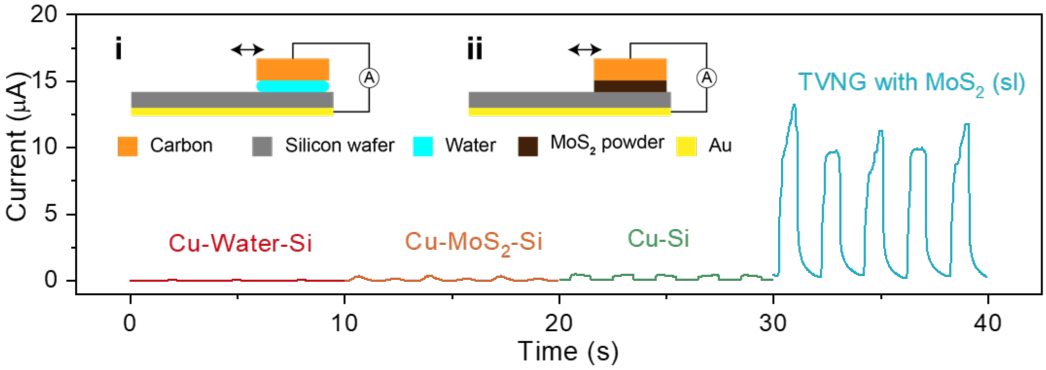

Figure S15. Output performance of TVNG with different structure (the inset (i) is the device with a water layer between Cu and Si, the inset (ii) is the device with a MoS_2 powder layer between Cu and Si).

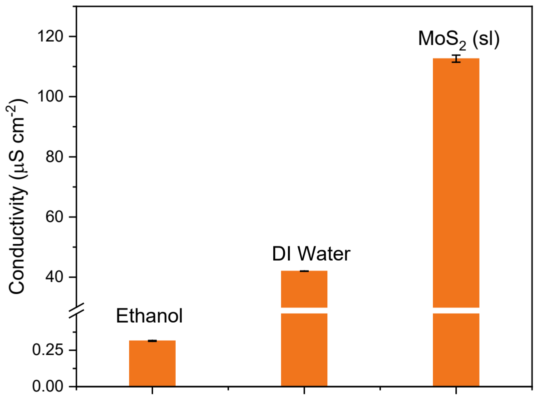

Figure S16. Conductivity of different interface optimization liquids.

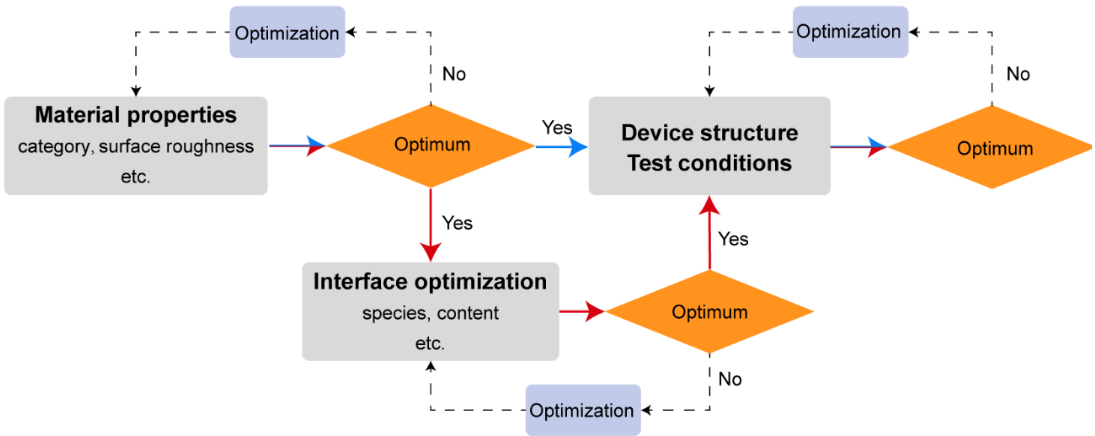

Figure S17. Design optimization flow for TVNG of the O-TVNG device.

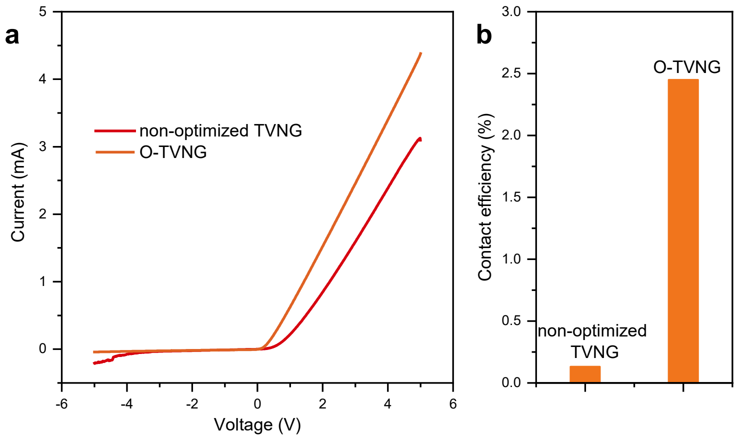

Figure S18. The (a) *I-V* curves and (b) corresponding contact area of O-TVNG and non-optimized TVNG.

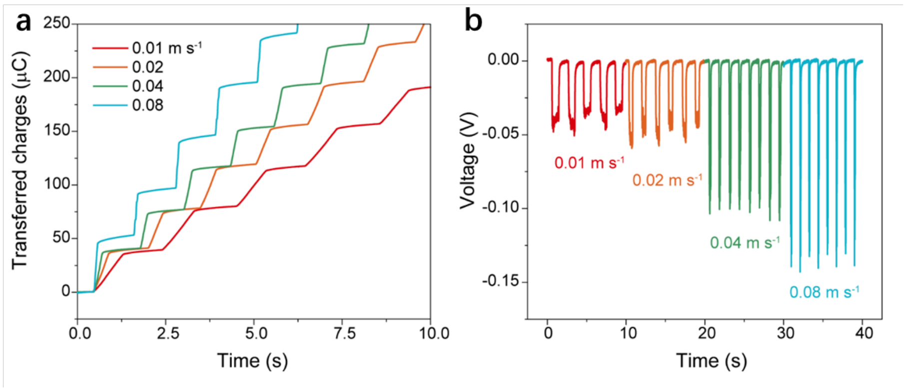

Figure S19. The (a) transferred charges, and (b) open-circuit voltage of O-TVNG under different sliding velocities (sliding distance: 1 cm).

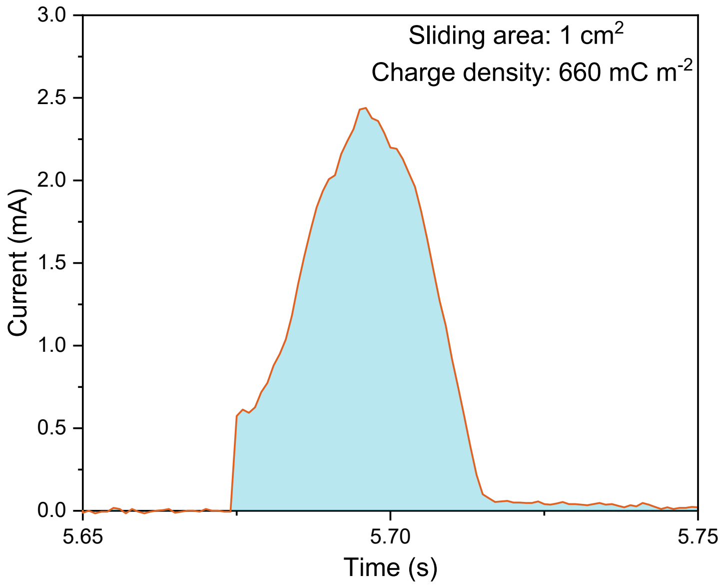

Figure S20. The calculation of transferred charges by current integration (accelerated speed: 10 m s^{-2}, sliding distance: 1 cm, and corresponding area: 1 cm^2).

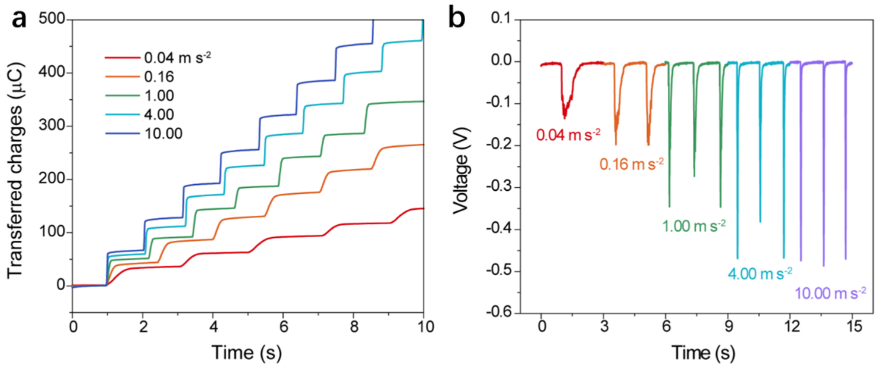

Figure S21. The (a) transferred charges, and (b) open-circuit voltage under different sliding accelerations (sliding distance: 1 cm).

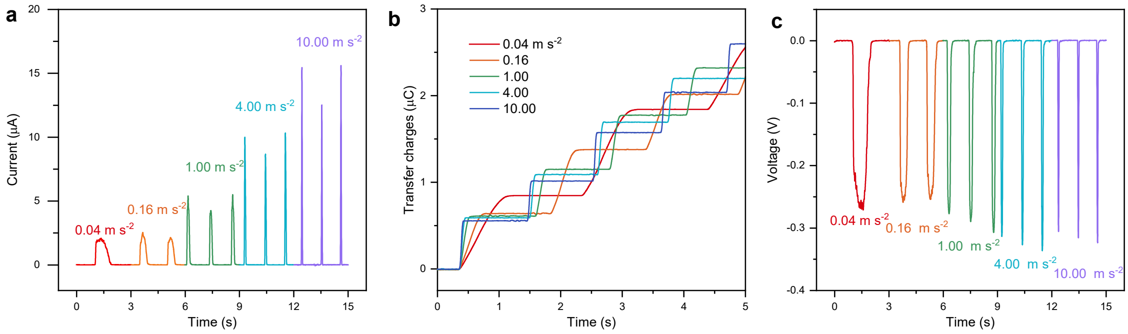

Figure S22. The (a) short-circuit current, (b) transferred charges, and (c) open-circuit voltage of non-optimized TVNG under different sliding acceleration (sliding distance: 1 cm).

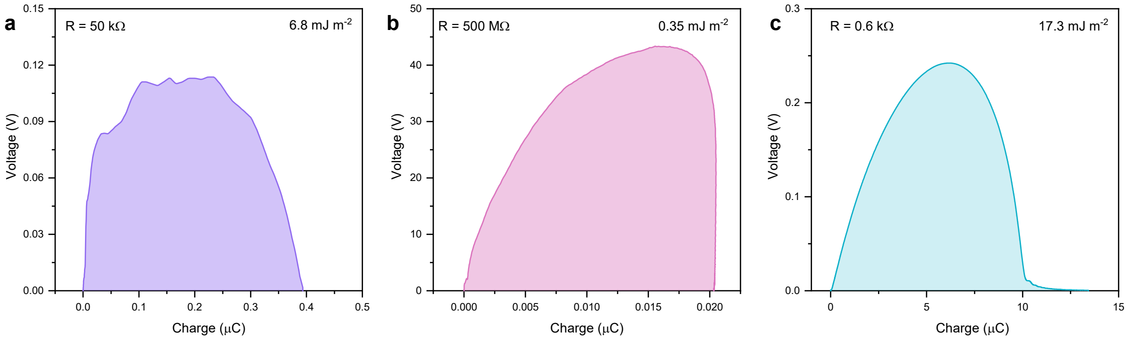

Figure S23. The energy density of (a) non-optimized TVNG, (b) sliding-mode TENG, and (c) O-TVNG under matched resistance, respectively, accelerated speed: 10 m s^{-2}, sliding distance: 1 cm, and corresponding area: 1 cm^2.

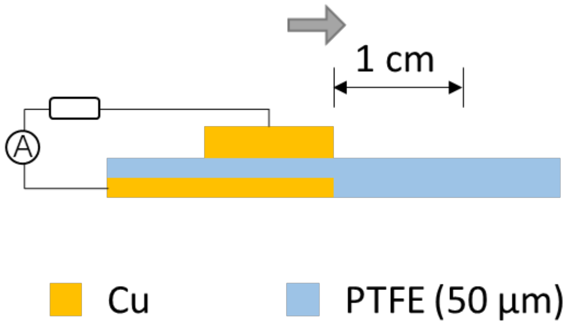

Figure S24. The schematic diagram of sliding-mode TENG.

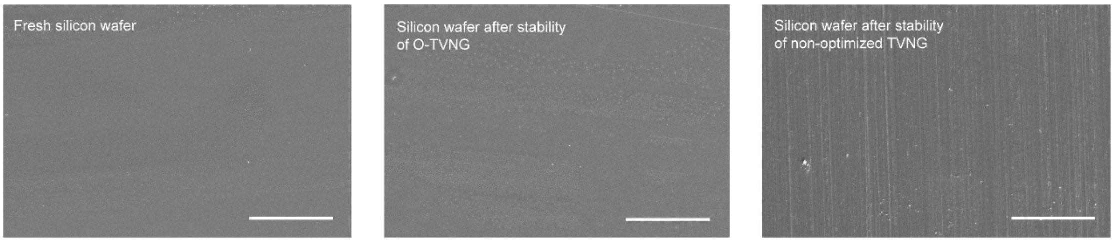

Figure S25. The scanning electron micrographs of silicon surface (scale bar: 30 μm).

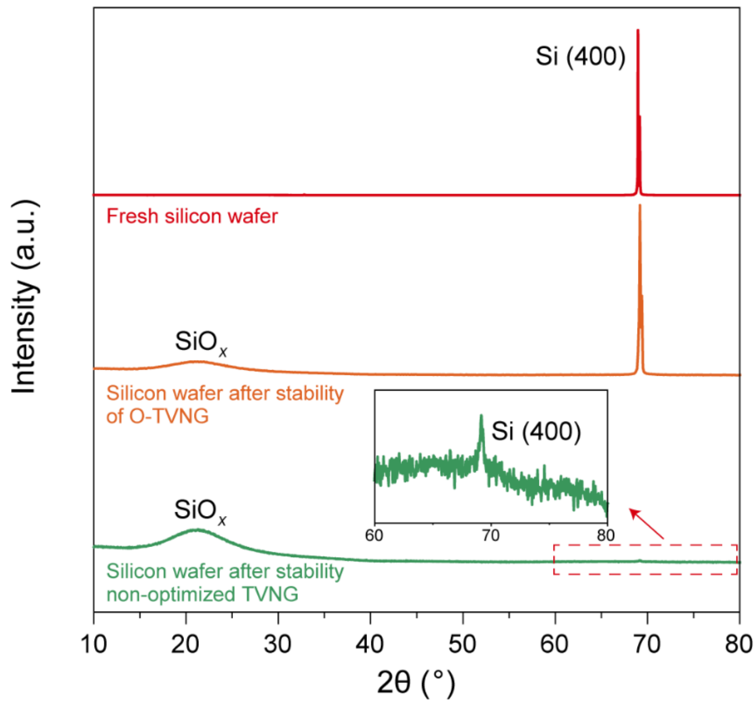

Figure S26. XRD patterns of silicon for TVNG before/after stability test.

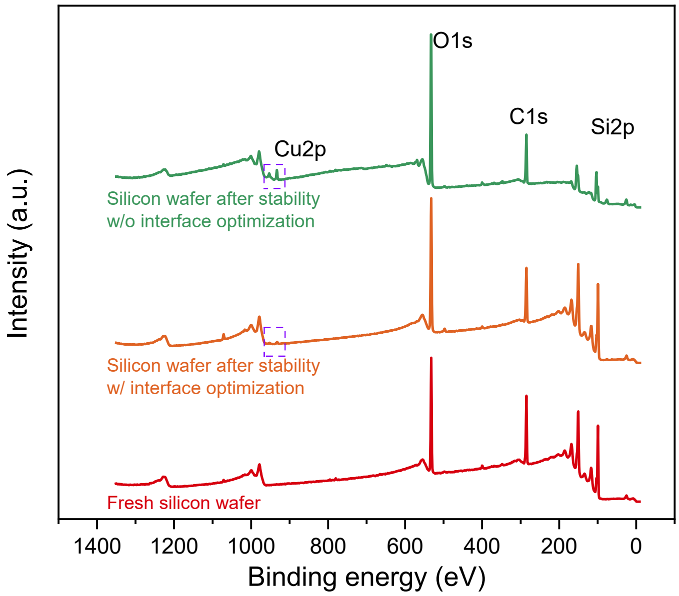

Figure S27. The XPS spectra of silicon surface.

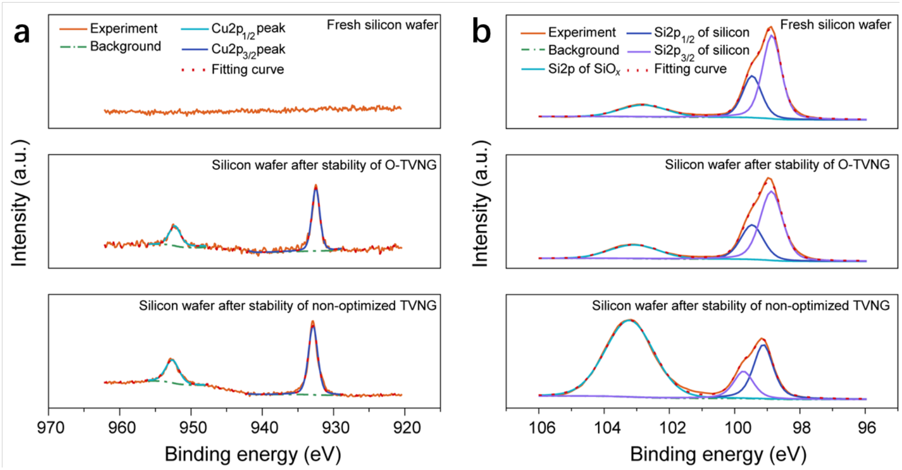

Figure S28. The (a) Cu2p spectra and (b) Si2p spectra of silicon for TVNG before/after the stability test.

Table S1. The turn-on voltage of TVNG under different pressure force according to the *I-V* curves in Figure 1c.

Force (N)	Turn-on voltage (V)
2	2.07
5	1.64
10	1.41
20	1.21

Table S2. The voltage (E_Q), current (I_Q) and resistance (R_Q) of quiescent operation point under different sputtering Cu areas according to the *I-V* curves in Figure S2.

Area (mm^2)	E_Q (V)	I_Q (A)	R_Q (Ω)
0.0625	3.36	1.63	2061.35
0.1250	3.23	1.77	1824.86
0.2500	3.05	1.96	1556.12
0.5000	2.95	2.05	1440.43
1.0000	2.87	2.13	1347.42
2.2500	2.8	2.2	1272.73
4.0000	2.71	2.28	1188.60
9.0000	2.67	2.32	1150.86
25.0000	2.63	2.35	1119.15

Table S3. The average R_Q and corresponding standard deviation of quiescent operation point under different sputtering Cu areas according to the different *I-V* curves (at least 5 curves are utilized to calculate the average R_Q).

Area (mm^2)	Average R_Q (Ω)	Standard deviation
0.0625	2022.18	131.57
0.1250	1878.34	43.01
0.2500	1567.51	17.15
0.5000	1439.38	29.44
1.0000	1352.98	9.63
2.2500	1229.25	31.00
4.0000	1186.65	11.96
9.0000	1139.91	15.51
25.0000	1101.01	18.97

Table S4. The R_Q, $R_{c,Cu}$, A_{eff}, and contact resistivity of TVNG device with/without interface optimization under different loading force.

	Force (N)	R_Q (Ω)	$R_{c,Cu}$ (Ω)	A_{eff} (mm^2)	Contact resistivity (Ω mm^2)
W/o interface optimization	2	3201	2141	0.016	34.30
	5	2517	1457	0.032	46.84
	10	2496	1436	0.035	51.11
	20	2355	1295	0.045	58.65
W/ interface optimization	2	1688	628	0.186	116.68
	5	1512	452	0.357	161.60
	10	1242	182	2.453	446.52
	20	1192	132	4.097	540.83

Note S1: The relationship between contact resistance and effective contact area for TVNG.

Considering a small region in the vicinity of the contact area, where has a thickness of Δx and contact area of A_c, as schematic in the following:

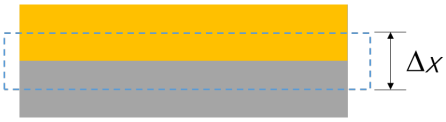

The relationship between contact resistance (R_c) and contact area can be calculated as follow:

$$R_c = \rho' \frac{\Delta x}{A_c} \tag{S1}$$

where the ρ' is the equivalent bulk resistivity of this region in the vicinity of the contact area (dotted box part in the insert). When the thickness of the region is thin enough, the contact resistivity ρ_c can be obtained:

$$\rho_c = \lim_{\Delta x \to 0} (\rho' \Delta x) = R_c A_c \tag{S2}$$

For a certain state of contact, the ρ_c is a constant. Thus, the R_c is inversely proportional to the A_c.

Note S2: The calculation of resistance of TVNG in quiescent operation point.

The Schottky contacts have non-linear characteristics (Figure 1c), the current varies with the voltage, causing a dynamic change in resistance under forward voltage. Thus, to calculate the resistance of TVNG in quiescent operation point (R_Q in Figure 1f), we use the graphic method to obtain the voltage and current at quiescent operation point ($R_Q = R_E + R_{con} + R_{c,Cu}$, where the R_E is the external resistance). The test circuit is shown in Figure 1f, we can measure the *I-V* curve (the orange curve in Figure 1f) of TVNG under an external resistance (R_E). Then, a loading line, whose *y*-intercept is E_d/R_E and *x*-intercept is E_d (E_d is the maximum value of external voltage source), is drawn. The point of intersection between *I-V* curve and loading line is the quiescent operation point (*Q*), and based on the corresponding voltage (U_Q) and current (I_Q), the quiescent operation resistance can be calculated according to Ohm's law $R_Q = U_Q/I_Q$.

Note S3: The influence of surface roughness on contact condition of TVNG.

As demonstrated in Figure S6-8, for the TVNG based on Cu and p-type silicon (unless otherwise specified, the Cu electrode area is always 1 cm^2, loading force is 10 N), the contact area decreases from 0.042 mm^2 to 0.011 mm^2 as the surface roughness of silicon increases from 0.5 ± 0.01 nm to 334.2 ± 26.9 nm (Figure S6 and S7). However, for the silicon, despite the surface roughness decrease by 668-fold, the contact area only increases by nearly 4-fold, indicating that macroscopic surface roughness decrease has limited significance in improving contact efficiency.

Note S4: The contact condition between Ga-In liquid metal and p-type silicon.

To investigate the contact condition between Ga-In and silicon, we measured the *I-V* curves of the Ga-In liquid metal and the p-type silicon. The circuit is shown in Figure S10a. As shown in Figure S10b, when the area of Ga-In is small, such as 2.8 mm^2, the *I-V* curves exhibit a rectification characteristic, indicating a Schottky junction, which is consistent with the previous reports[S1,S2]. However, as the area of Ga-In increases, the rectification characteristic becomes weaker, and when the area of Ga-In is larger than 37.5 mm^2, the *I-V* curves are hardly distinguishable from the linear *I-V* curve of an Ohmic junction. When an external resistance of 1 kΩ is connected in the circuit, it can be seen that only the sample with 2.8 mm^2 shows a clear rectification characteristic, as shown in Figure S10c. The rest of the samples show linear *I-V* curves with the external resistance of 1 kΩ. However, when the Ga-In liquid metal is used in TVNG, it tends to spread on the surface of the silicon wafer. The area of the spread Ga-In on the silicon surface is very large. Therefore, the rectification characteristic is not observed under 1 kΩ external resistance, as shown in Figure 2a.

Note S5: The difference of contact condition between TVNG with and without interface optimization methods.

As shown in Figure S14, compared to the TVNG without interface optimization methods (Figure S1), the optimized contact efficiency of the TVNG significantly enhances its output, particularly at the weak loading of 5 N, the output of the TVNG increases by 142-fold, from 0.04 μA to 5.78 μA. However, the effective contact area only increases by 11.1-fold, from 0.032 mm^2 to 0.357 mm^2.

Note S6: Contribution of the friction between MoS_2 and Cu/silicon, and the friction between liquid and Cu/silicon for the output of TVNG.

When the MoS_2 liquid is filled at the interface, the interfacial material type is complex. There are some potential friction processes that will occur when the Cu electrode slides on the silicon, such as MoS_2/Cu, liquid/Cu, MoS_2/Si, or liquid/Si. To confirm the influence of these friction processes, we measured the charge transfer process of TVNG with different structures, as shown in Figure S15.

To study the effects of the friction between liquid and Cu/silicon, we designed a TVNG device whose structure is shown in the inset (i) of Figure S15. For this structure, the Cu electrode does not contact the silicon, and the corresponding gap is filled with water and the thickness of the water layer is about 0.5 mm. When the Cu electrode slides over the silicon, there is almost no current signal output in the external circuit (Figure S15), indicating that the friction process between liquid and Cu/Si has a negligible influence on the output.

To investigate the effects of the friction between MoS_2 and Cu/silicon, we designed another TVNG device whose structure is shown in the inset (ii) of Figure S15. For this structure, the Cu electrode also does not contact the silicon, and the corresponding gap is filled with MoS_2 powder and the thickness of the MoS_2 powder layer is about 0.5 mm. When the Cu electrode slides over the silicon, there is a small current signal output in the external circuit (Figure S15), which is lower than the output of TVNG with Cu and Si. This suggests that the friction process between MoS_2 and Cu/Si also has a minor influence on the output.

However, when the MoS_2 (sl) is added to the TVNG with Cu and Si, its current output can be dramatically improved, as shown in Figure S15. In addition, it is obvious that the output of TVNG with MoS_2 (sl) is nearly 20 times higher than the sum of the output of TVNG with Cu and Si, the output between MoS_2 and Cu/silicon, and the output between water and Cu/silicon. Thus, the contribution of the friction between MoS_2 and Cu/silicon, and the friction between water and Cu/silicon to the huge output enhancement of TVNG with MoS_2 (sl) is very weak.

Note S7: The design optimization strategy for TVNG device.

To enhance the contact efficiency of TVNG based on the improved approaches and mechanisms, and achieve high-performance devices, we propose a design optimization strategy, as shown in Figure S17. This strategy consists of two parts. The blue line in the flow diagram represents the optimization method for conventional TVNG, which only includes the screening of material pairs, the optimization of surface properties (such as roughness), and the refinement of device structure and test conditions. However, in our work, we provide a more comprehensive optimization strategy, as indicated by the red line in the flow diagram. On top of the conventional strategy, we add the crucial interface optimization with the selection or adjustment of interface materials. This approach leads to the development of optimized TVNG (O-TVNG) devices with significantly higher contact efficiency and better output performance.

Note S8: The surface characteristics of silicon before/after long-term operation.

As shown in the X-ray diffraction (XRD) results (Figure S26), a heavily oxidized phenomenon can be observed, accompanied with an amorphous peak around 20° and tiny crystallization (400) peak for p-type silicon, but the interface optimization strategy can alleviate this phenomenon. The X-ray photoelectron spectroscopy (XPS) results show that the material transition content of the O-TVNG is much less than that of the non-optimized TVNG (Figure S27 and Figure S28). The O-TVNG also has a weaker oxidized peak according to Si2p spectra, which aligns with the XRD results, as shown in Figure S28. These results demonstrate that the design optimization approach can reduce wear, ensure good contact efficiency, and protect the semiconductor surface properties, thus ensuring the stability of TVNG performance.

References

[S1] H. Reichert, M. Denk, J. Okasinski, V. Honkimäki, H. Dosch, Giant metal compression at liquid-solid (Pb-Si, In-Si) Schottky junctions, Phys. Rev. Lett. 98(11) (2007) 116101.

[S2] S. Arscott, M. Gaudet, Electrowetting at a liquid metal-semiconductor junction, Appl. Phys. Lett. 103(7) (2013) 144101.